Journal of Energy Chemistry, Vol. 26, Issue 5, September 2017, pp. 891-901
DOI:10.1016/j.jechem.2017.07.014

Copper-based oxygen carriers supported with alumina/lime for the chemical looping conversion of gaseous fuels

Syed K HAIDER[1*], María ERANS[1], Felix DONAT[3], Lunbo DUAN[1,2], Stuart A SCOTT[3], Vasilije MANOVIC[1], Edward J ANTHONY[1]

[1] *Combustion and CCS Centre, Cranfield University, Bedfordshire, MK43 0AL, UK*

[2] *Key Laboratory of Energy Thermal Conversion and Control, Ministry of Education, School of Energy and Environment, Southeast University, Nanjing, 210096, China*

[3] *Department of Engineering, University of Cambridge, Trumpington Street, Cambridge, UK*

**Corresponding author, haidersyedkumail@gmail.com*

Abstract – Copper (II) oxide in varying ratios was combined with either an alumina-based cement (Al300), or CaO derived from limestone as support material in a mechanical pelletiser. This production method was used to investigate its influence on possible mechanical and chemical improvements for oxygen carriers in chemical looping processes. These materials were tested in a lab-scale fluidised bed with CO or CH_4 as a reducing gas at 950 °C. As expected, the oxygen carriers containing a greater ratio of support material exhibited an enhanced crushing strength. Oxygen carriers comprised of a 1:3 ratio of support material to active CuO exhibited increased crushing strength by a minimum of 280% compared to pure CuO pellets. All oxygen carriers exhibited a high CO conversion yield and were fully reducible from CuO to Cu. For the initial redox cycle, Al300-supported oxygen carriers showed the highest fuel and oxygen carrier conversion. The general trend observed was a decline in conversion with an increasing number of redox cycles. In the case of CaO-supported oxygen carriers, all but one of the oxygen carriers suffered agglomeration. The agglomeration was more severe in carriers with higher ratios of CuO. Oxygen carrier Cu25Al75 (75% wt. aluminate cement and 25% wt. CuO), which did not suffer from agglomeration, showed the highest attrition with a loss of approximately 8% of its initial mass over 25 redox cycles. The reducibility of the oxygen carriers was limited with CH_4 in comparison to CO. CH_4 conversion yielded 15-25% and 50% for Cu25Ca75 (25% wt. CuO and 75% wt. CaO) and Cu25Al75, respectively. Cu25Ca75 demonstrated improved conversion, whereas Cu25Al75 exhibited a trending decrease in conversion with increasing redox cycles.

1 Introduction

Chemical looping combustion (CLC) is a highly efficient fuel-processing technology with inherent CO_2 separation. The resulting flue gas from the process is rich in CO_2, which can be utilised or compressed and stored. The technology's greatest advantage is its ability to separate oxygen from combustion air and utilise it directly in the conversion of a carbonaceous fuel. This process can avoid the otherwise necessary post-combustion flue gas treatment and energy penalty associated with conventional combustion taking place in air [1]. CLC systems are typically comprised of two interconnected fluidised bed reactors, denoted as a fuel reactor and air reactor with a recirculating oxygen carrier. This oxygen carrier (typically a transition metal oxide) allows the conversion of the carbonaceous fuel, be it gas [2], liquid [3] or a solid fuel [4]. A simplified CLC process is shown in Figure 1. The two fluid beds are abbreviated as AR for the air reactor and FR for the fuel reactor. In the FR the oxidised oxygen carrier provides the necessary oxygen for the fuel conversion, allowing for combustion products to be formed as the flue gas. The now reduced oxygen carrier is transferred to the AR where it is then re-oxidised, allowing the cyclic process to continue [5].

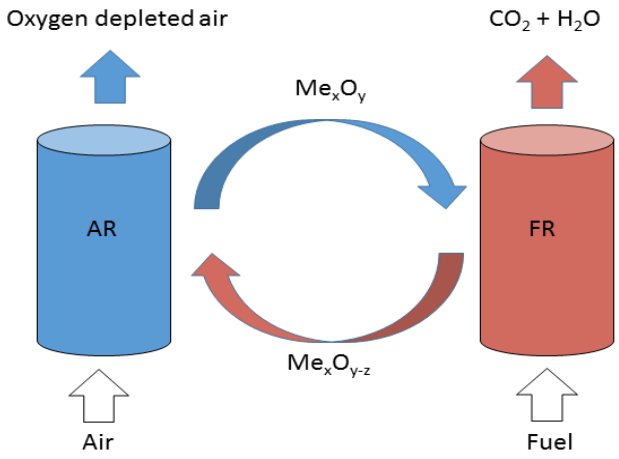

Figure 1: Simplified CLC process, adapted from [5]

With the maturity of fluidised bed technology established as an important means of fuel processing, CLC requires a suitable and stable oxygen carrier for the process to be employed at larger scales. Oxygen carrier research has been prolific since 2001 with many candidate materials tested [6].

Copper-based materials have been studied as potential oxygen carriers for the chemical looping process in great detail [7–12]. Copper-based systems have favourable redox characteristics, where both the oxidation and reduction reactions are exothermic; they also possess a high oxygen transfer capacity. Furthermore, copper systems can decompose to a lower metal oxidation state liberating gaseous oxygen at low oxygen potentials and is known as the chemical looping with oxygen uncoupling (CLOU) process [13]. The gaseous oxygen released in the CLOU process can greatly enhance the oxidation of char by avoiding the

necessity of the char to be gasified into a synthesis gas for combustion in the conventional CLC process.

Examples of the benefits provided by the CLOU properties of a copper-based system are demonstrated by the fact that the conversion rate of a solid fuel, for example petroleum coke, can be increased by a factor of 80 times [14] compared to conventional solid fuel CLC. This faster rate of conversion can reduce the requirement of the solids inventory and total reactor volume for a given fuel feeding rate and, hence, reduce the associated capital and operational costs of a CLC process [9]. It has been calculated that the amount of oxygen carrier per MW_{th} of input fuel could be reduced to approximately 135 kg using CuO. By contrast, one would require approximately 1200 kg per MW_{th} of fuel input for Fe_2O_3 operating in conventional CLC process [15]. Like all oxygen carriers in the fluidised bed process, these carriers are subjected to mechanical and chemical reaction stresses. In terms of CuO-based oxygen carriers, the copper oxide component is far more costly than some alternatives, for example, they are likely to cost about 10 times more than a comparable iron oxide carrier [6]. It is, therefore, imperative that the material inventory losses associated with attrition should be minimised. Attrition resulting from both mechanical and chemical reaction stresses can be significantly reduced by the appropriate choice of a support material for the active phase, as well as by the choice of the method of preparation of the oxygen carrier. However, all methods of oxygen carrier preparation must be scalable in order to produce the quantities required in full-scale operation. Also, the material utilised as a support should be of relatively low cost to ensure the overall cost of the produced oxygen carrier is minimised.

This investigation consisted of an experimental study, in which CuO as the active phase was produced as an oxygen carrier in varying ratios with a low-cost support material, consisting of CaO derived from a natural limestone, or alumina-based cement. The oxygen carriers produced were characterised through means of X-ray diffraction spectroscopy (XRD), scanning electron microscopy (SEM) with energy-dispersive X-ray spectroscopy (EDX), crushing strength and measurement of bulk density. Their assessment through these characterisation techniques helped determine their suitability in a CLC process. The oxygen carriers were then investigated for their efficacy for gaseous fuel conversion. This was assessed in a cyclic redox investigation with CO as a reducing gas in a lab-scale fluidised bed reactor. The oxygen carriers showing better suitability were finally further investigated for their reactivity and conversion of CH_4.

2 Experimental

2.1 Materials

The support material for the oxygen carriers produced was CaO, which was obtained from the calcination of limestone from Longcliffe (UK), or an alumina-based cement, traded as ‘Alpha-bond 300’, sourced from Almatis GmbH (Germany) and referred to as Al300. The CuO was obtained from Johnson Matthey (UK). The produced series of oxygen carriers had varying weight ratios of CuO with either the CaO or alumina-based cement as the support material. The detailed compositions of the support materials are given in Table 1.

Table 1: Properties of reagents used in oxygen carrier preparation

	CuO Johnson Matthey	**Alumina-based cement (Almatis) 'Alpha-bond 300'**	**Limestone Longcliffe (UK)**
Composition	CuO (min~98%)	Al_2O_3 (min~88%) CaO (max~0.1%) Na_2O (max~0.5%) SiO_2 (max~0.3%)	$CaCO_3$ (min~98%)
Particle size (as received)	120 μm (100% passing) 70 μm (20% passing)	90 μm (max~30%) 50 μm (min~4%) 50 μm (max~8%)	600 μm (100% passing) 425 μm (85-95% passing) 300 μm (60-85% passing) 212 μm (30-50% passing) 150 μm (10-20% passing) 45 μm (min~4%)
Particle size (After crushing in ball mill)	80% 10 μm or less (Malvern Mastersizer 2000)		

2.2 Particle production

The reagents used in this investigation were of too large particle size to be used as received. Therefore, prior to the production of the oxygen carriers, the reagents were crushed in a ball mill (Orto-Alesa). The defined ratio of copper and support material (totalling 1 kg) were added to the ball mill drum along with 1 kg of 10 mm hardened stainless steel ball bearings. The ball mill was operated for 24 h at 100 rpm. The production method of oxygen carriers explored in this work was based on a pelletisation method [16], which utilised a table-top TGM granulator manufactured by Glatt.

The mechanical mixing manufacturing method was employed here for its scalability as well as its economy for resources and lower costs compared to other production techniques. In comparison to methods such as freeze granulation, co-precipitation, sol-gel and wet impregnation, mechanical mixing offers a greater degree of scalability and reduction in waste products from the manufacturing process [17]. Typically, copper-based oxygen carriers are not suited to being produced by mechanical mixing due to poor mechanical strength. However, the granulation production method is shown to work well in producing calcium looping sorbents [18,19] and could offer a scalable and economic method for producing copper-based oxygen carriers with robust supports including CaO, that have the potential for enhanced mechanical properties.

The granulator consists of a mixing vessel, in which high-shear rotating blades are mounted horizontally and vertically. These blades are designated the agitator and chopper, respectively. The fine powdered reagents produced in the ball mill were weighed to the desired quantities. Then, they were transferred to the mixing vessel. The rpm of the agitator and the chopper were set to 500 and 2500, respectively. Water was then added to the powdered mixture, introduced through a pressurised spray nozzle system which could be turned on or off as

desired. The water spray was added for 10 s at intervals of 60 s. After each minute, the process was discontinued to visually inspect the mixture to ensure no over-saturation and correct grain size. The effect of over-saturation in a short period of time would lead to particle sizes larger than those desired.

When Al300 was the support material, approximately 150-200 mL of water was added per kg of powdered mixture. When CaO was used as the support, the addition of water causes the formation of $Ca(OH)_2$ in an exothermic reaction. Therefore, a greater quantity of water was required to form the pelletised oxygen carriers due to the loss of water through evaporation from the heat released from the reaction. The extent of water loss varied strongly with the % wt. ratio of CaO used as a support. Typically, between 300-500 mL of water was added per kg of powdered material. The formed particles were then transferred to an alumina tray for air-drying at 200 °C. The particles were then sintered at 900 °C in a furnace for 4 h. Following the sintering step, the pelletised oxygen carriers were sieved to the desired size range of 355-425 μm.

The oxygen carriers produced by the pelletisation technique were effectively spherical, making them suitable for fluidised bed operation. However, the size range of oxygen carrier was dictated by a combination of time in the granulator and the quantity of water added. With the correct management of water addition and time, one batch can typically produce 60% of particles in the required size range. In particular, Cu based carriers are always prepared with a support material to avoid problems with sintering and potential attrition []

2.3 Oxygen carrier characterisation

The produced oxygen carriers were characterised by X-ray diffraction crystallography (XRD) by means of a Siemens D5005 (2θ =10-90º) and by scanning electron microscopy (SEM) Philips XL30 with Schottky Field Emission Gun (SFEG) mode for high-resolution imaging. The SEM was also coupled with energy-dispersive X-ray (EDX) spectroscopy analysis by Oxford Instruments Swift-ED and analysed by Aztex systems software. The crushing strength of the particles was determined by a Shimpo FGN-5 load cell, which is applicable for particles in a size range between 325-425 μm.

2.4 Experimental setup and conditions

The investigation into gaseous fuel conversion was conducted in a quartz fluidised bed reactor (FBR) heated by an external furnace as shown in Figure 2. The reactor height was 550 mm with an internal diameter of 24 mm. The distribution plate consisted of sintered porous quartz (porosity grade 1) and was located 100 mm above the bottom of the reactor. The FBR utilised mixtures of N_2 and air, N_2, CO 10% in N_2 balance and CH_4 5% in N_2 balance, all supplied from gas cylinders from BOC Ltd using three Bronkhorst (EL-FLOW series) mass flow controllers to control the flow rate. A portion of the exhaust gases from the FBR was sampled continuously by a means of a pump using an approximate flow rate of 0.5 L min^{-1} through a 6.25 mm OD stainless steel tube inserted 100 mm into the top of the quartz reactor. A particle filter protected the downstream analysis equipment and a moisture trap with a $CaCl_2$ drying agent, which ensured the gas sample was dry. The sampled gas was analysed at a frequency of 1 Hz by an ABB EL3020 series multi gas analyser, which measured the gas flows of CO,

CO_2, CH_4 (0-20 vol%) and O_2 (0-25 vol%). Temperature measurements of the bed were made with a K-type thermocouple inserted into the fluidised bed reactor. The differential pressure was measured across the bed using an Omega PX138 pressure transducer to ensure the bed was fluidised throughout the investigations.

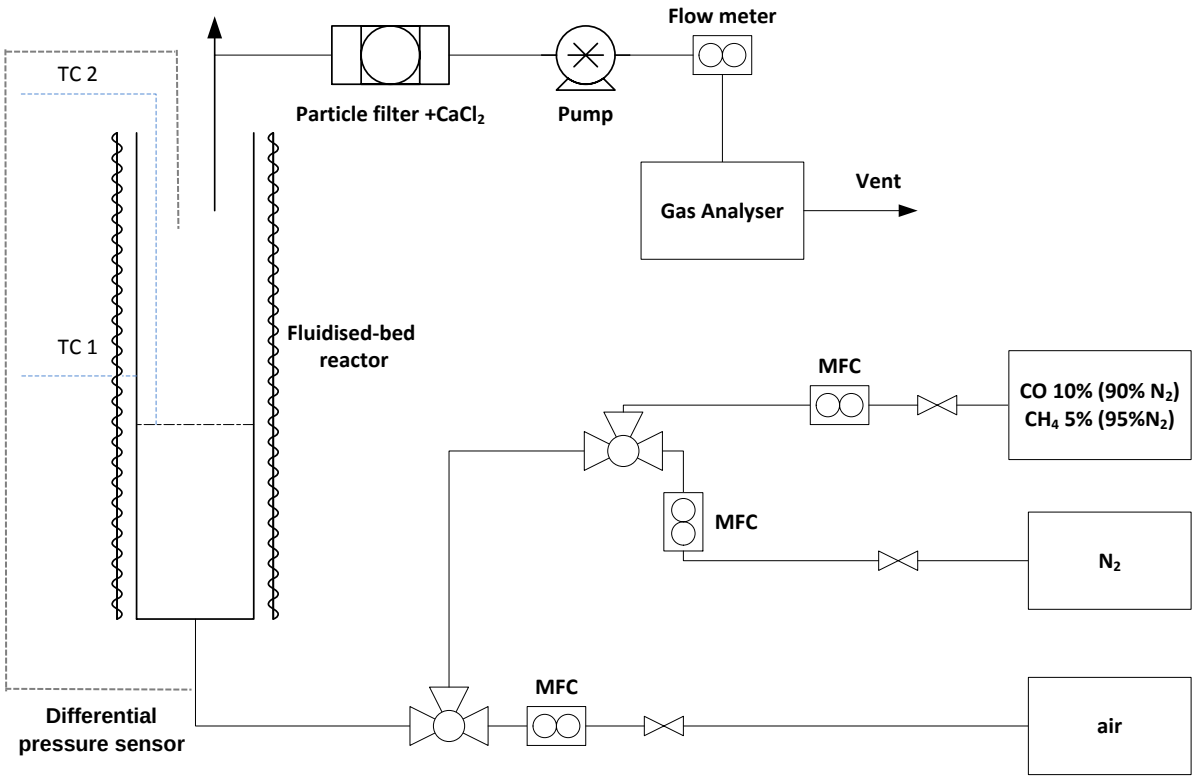

Figure 2: Simplified scheme of fluidised bed reactor for redox investigation

The experimental setup described above was used to investigate the cyclic performance of oxygen carriers with varying ratios of CuO as the active phase supported by either CaO or Al300. The oxygen carriers were fluidised in the bubbling regime and were subjected to 25 redox cycles. All investigations were conducted at 950°C. As both the oxidation and reduction reactions of CuO/Cu_2O are exothermic, the oxygen carrier was diluted with silica sand (325-450 μm from Sigma Aldrich) in order to help control the bed temperature. In the investigation, approximately 1.5 g of oxygen carrier was used together with 13.5 g of silica sand. A blank cycle was conducted with sand only for calibration of the analysers and to determine whether there were any side reactions of the reactor material with the oxidation and reduction gases. Each redox cycle consisted of 4 stages: 1) inert stage with N_2 for a period of 300 s, 2) reduction stage with CO 10% in N_2 balance or CH_4 5% in N_2 balance for a period of 60 s, 3) sweeping stage with N_2 for 60 s, 4) oxidation stage with air 20% with N_2 balance for 360 s. The air in the oxidation stage was diluted with nitrogen to give an O_2 concentration of 5%. The rate of the oxidation phase in copper-based oxygen carriers is rapid. Using an oxidation period of 360 s ensures and assumes that the oxygen carrier is fully oxidised prior to the subsequent inert and reduction phases. The inlet gas flows were maintained at a combined 30 mL s^{-1} measured at standard conditions (20 °C and 101.3 kPa) for all the gaseous reaction environments. This corresponded to a ratio of superficial fluidising gas velocity (U_0) to

minimum fluidisation velocity (U_{mf}) of approximately 4, giving rise to a vigorously bubbling bed. The gaseous operating conditions are listed in Table 2.

Table 2: Experimental conditions, gases and flow rates

Condition	Gas composition	Time (s)	Gas flowrate (L min^{-1})	Temperature (°C)
Inert	N_2	300	1.8	950
Reduction	10% CO (N_2 balance)	60	1.8	950
	5% CH_4 (N_2 balance)			
Inert	N_2	60	1.8	950
Oxidation	5% O_2 (20% air, N_2 balance)	360	Air 0.45	950
			N_2 1.35	

2.5 Data evaluation

The degree of oxygen carrier conversion (X) in this investigation is defined in Equation 1 and is used to describe the extent to which the oxygen carrier can be reduced. (m) is the mass of the sample at a given time (i), (m_{red}) is the mass of the fully reduced sample and (m_{ox}) is the mass of the fully oxidised sample.

$$X = \frac{m_i - m_{red}}{m_{ox} - m_{red}} \qquad \textit{Equation 1}$$

(X_{red}) is used to determine the mass-based conversion across a fuel reduction cycle and is defined for CH_4 and CO in Equation 2 and Equation 3, respectively. ($P_{i,out}$) is the concentration of the gaseous species leaving the reactor, ($n_{tot,in}$) is the total number of gaseous moles entering the reactor in mol s^{-1}, (M_{CuO}) is the molecular weight of CuO in g mol^{-1}. (a_{oc}) is the mass fraction of active metal oxide in the oxygen carrier and (m_{oc}) is the mass of the oxygen carrier sample. The yield of gas conversion (γ) can be calculated with Equation 4 and Equation 5, where P_i denotes the partial pressure of the gaseous component i [20].

$$X_{red} = X_{red-1} - \int_{t_{-1}}^{t} \frac{n_{tot,in} \cdot M_{CuO}}{m_{OC} \cdot a_{OC}} \cdot \left(4P_{CO_{2,out}} + 3P_{CO_{out}} + 2P_{O_{2,out}}\right)dt \qquad \textit{Equation 2}$$

$$X_{red} = X_{red-1} - \int_{t_{-1}}^{t} \frac{n_{tot,in} \cdot M_{CuO}}{m_{OC} \cdot a_{OC}} \cdot \left(2P_{CO_{2,out}} + P_{CO_{out}} + 2P_{O_{2,out}}\right)dt \qquad \textit{Equation 3}$$

$$\gamma_{CH_4} = \frac{P_{CO_2}}{P_{CO_2} + P_{CO} + P_{CH_4}} \qquad \textit{Equation 4}$$

$$\gamma_{CO} = \frac{P_{CO_2}}{P_{CO_2} + P_{CO}} \qquad \textit{Equation 5}$$

3 Results and Discussion

3.1 Particle characterisation

Table 3 shows the crushing strength, bulk (tapped) density and the major crystalline phases seen in the freshly pelletised oxygen carriers. The crushing strength was improved with increasing amounts of support material in the oxygen carrier. The average crushing strength of thirty pure CuO particles was 0.43 N; in comparison to oxygen carriers containing the lowest percentage of support material, the crushing strength improved by a minimum of 280%.

Table 3: Oxygen carrier characterisation properties

Name of OC	Crushing strength (N)	Bulk (tapped) density (kg m^{-3})	Major crystalline phases
Cu25Al75	1.55	1680	Bohmite, Tenorite
Cu50Al50	1.27	2680	Corundum, Tenorite
Cu75Al25	1.23	3510	Corundum, Tenorite
Cu25Ca75	1.63	2220	Portlandite, Tenorite
Cu50Ca50	1.50	2219	Portlandite, Tenorite
Cu75Ca25	1.31	3320	Portlandite, Tenorite, Ca_2CuO_3 (orthorhombic)

The major crystalline phases in the produced oxygen carrier particles were determined by XRD spectrometry. Their diffraction spectra are shown in Figure 3 and Figure 4 for Al300 and CaO supports, respectively. There are no significant differences between phases seen in the diffraction spectra, with exceptions in Cu25Al75 where the presence of Bohmite was identified, which typically should not be present, when the samples were calcined at 900^{o}C but was still identified. In CaO supported samples, Portlandite was present in all samples, indicating the samples may have absorbed some atmospheric moisture in storage. The Cu75Ca25 oxygen carrier saw the presence of a copper calcium compound Ca_2CuO_3, which has been reported in previous studies [9].

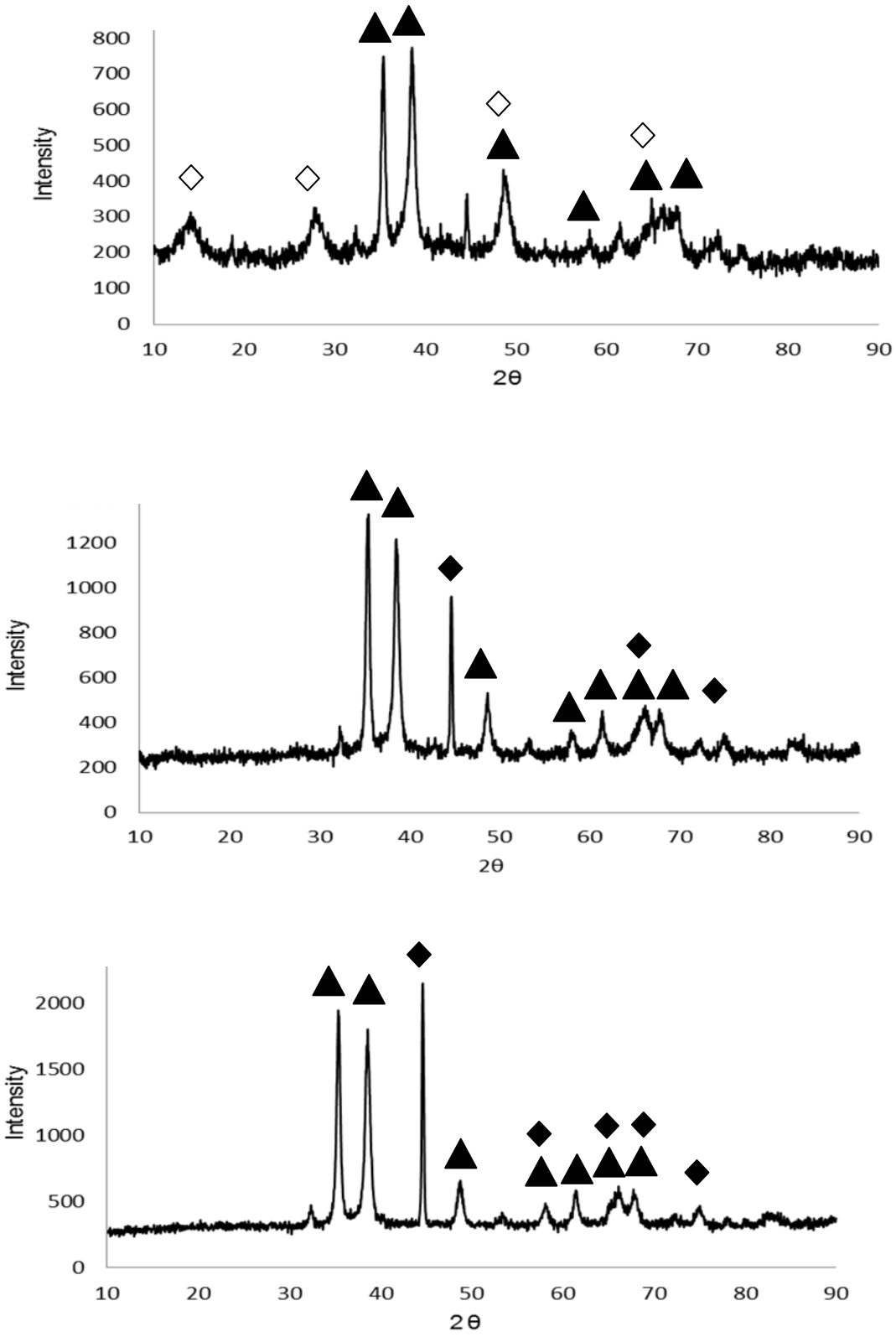

Figure 3: XRD spectra of alumina-supported oxygen carriers (Top)-Cu25Al75 (Centre)-Cu50Al50 (Bottom)-Cu75Al25 ▲-CuO (Tenorite) ♦- Al_2O_3 (Corundum) ◊-AlO(OH) (Bohmite)

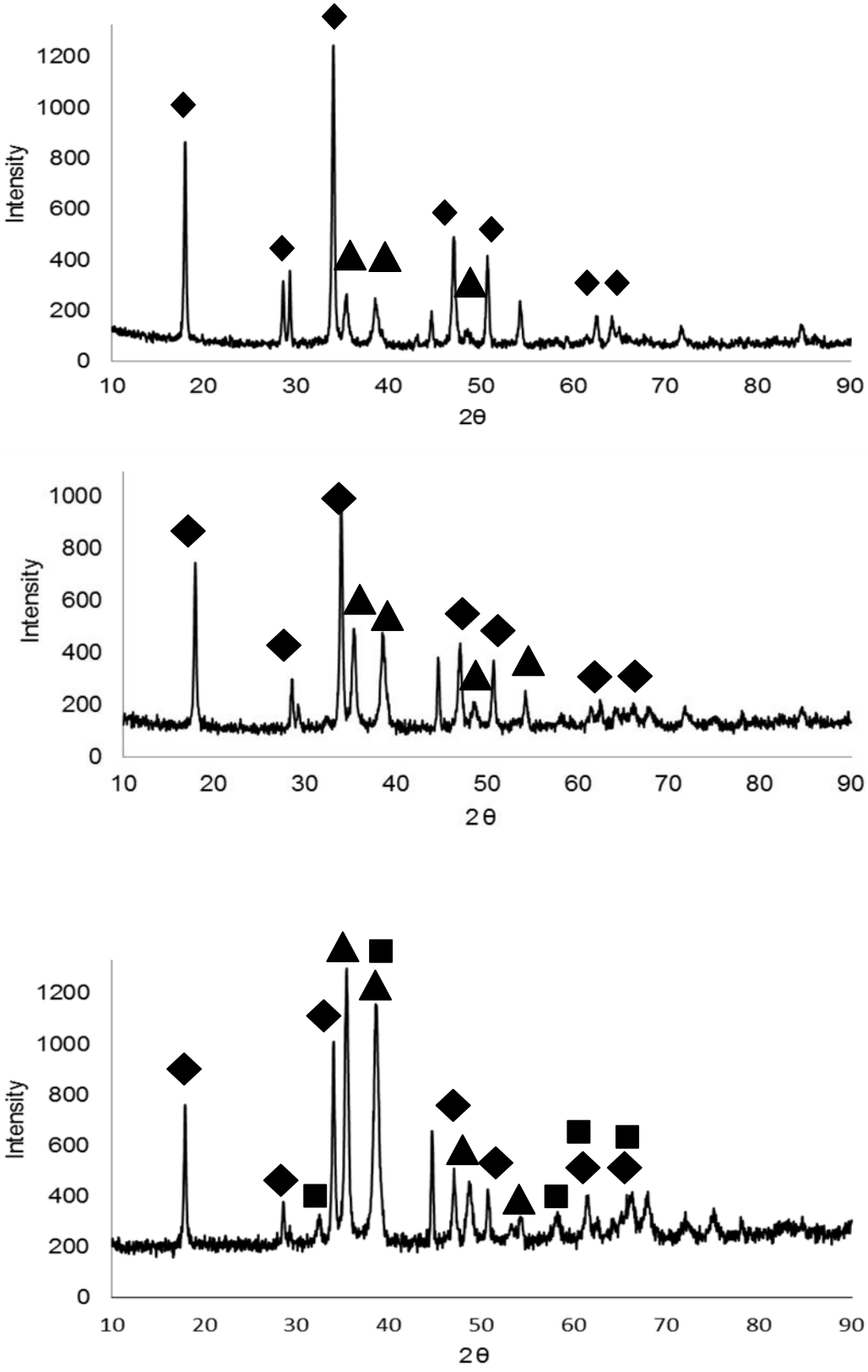

Figure 4: XRD spectra for Ca-supported oxygen carriers (Top)-Cu25Ca75 (Centre)-Cu50Ca50 (Bottom)-Cu75Ca25 ▲-CuO (Tenorite) ♦-$Ca(OH)_2$ (Portlandite) ■-Ca_2CuO_3

The freshly prepared particles were assessed under SEM in SFEG mode for high-resolution imaging. To investigate the internal composition of the oxygen carriers, the particles were first mounted on an epoxy resin. This resin mould was then ground back to reveal the cross-sectional area of the particles. The resin moulds were then assessed under SEM with EDX analysis. This allowed the examination of the uniformity of support material and copper (II) oxide within.

The oxygen carriers containing the Al300 support are shown in Figure 5-7. The non-uniformity of the elemental distribution within the particles shows that the CuO tends to be localised to specific areas within a given particle. This is also observed in the oxygen carrier particles containing CaO as a support (Figure 8-10).

The comparison in morphology of the 25% CuO-containing oxygen carriers clearly shows a difference in support material structure. In Cu25Al75 (Figure 4ii) it appears the Al300 supports were formed of smaller particles and are compacted together with the CuO to form the oxygen carrier. In contrast to the Cu25Ca75 (Figure 7ii), the formation of the CaO support appears to be uniform with a greater distribution of the active CuO and the increased connectivity with the support is likely a contributing factor for its increased crushing strength over the Al300-supported particles. In the Cu75Ca25 oxygen carrier XRD indicated the presence of Ca_2CuO_3 and this may be present in all the CaO-supported samples, although not as a major identified phase. This mixed compound has a low melting point [9] which could bond particulates and contribute to the increased crushing strength. The pelletisation method favours the use of CaO as a support material. It can be seen that the CaO-supported oxygen carriers (Figures 8i, 9i and 10i) appear to be more spherical than the Al300-based particles (Figures 5i, 6i and 7i) and can result in more favourable fluidisation properties and less attrition due to reduced fragmentation and ‘rounding’ of the particles occurring during fluidising operation due to the removal of asperities on the particles.

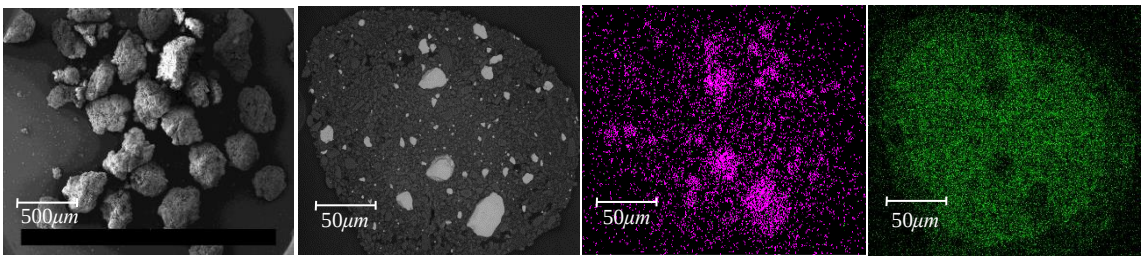

Figure 5: Cu25Al75 i) High-resolution SFEG image (scale 500 µm), ii) Global particle view EDX, iii) Cu elemental mapping EDX, iv) Al elemental mapping EDX

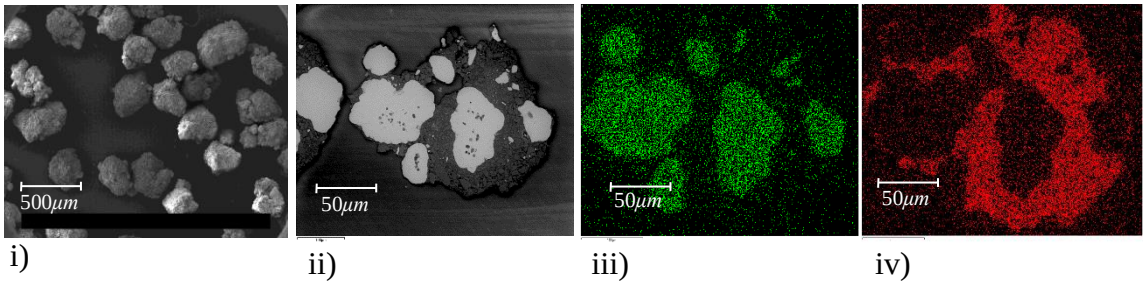

Figure 6: Cu50Al50 i) High-resolution SFEG image (scale 500 µm), ii) Global particle view EDX, iii) Cu elemental mapping EDX, iv) Al elemental mapping EDX

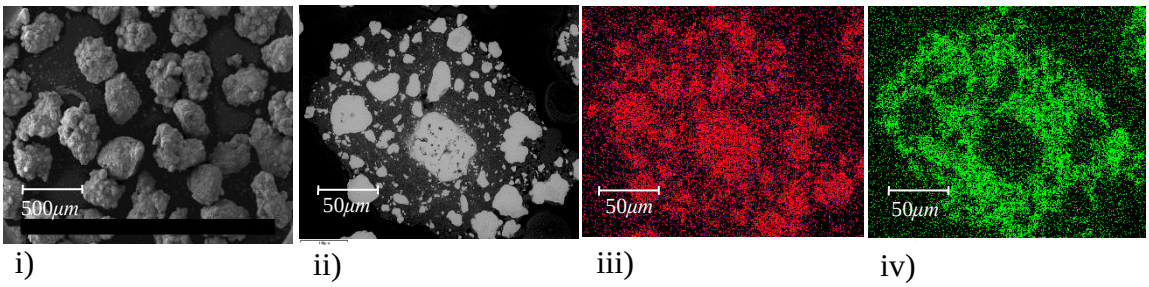

Figure 7: Cu75Al25 i) High-resolution SFEG image (scale 500 µm), ii) Global particle view EDX, iii) Cu elemental mapping EDX, iv) Al elemental mapping EDX

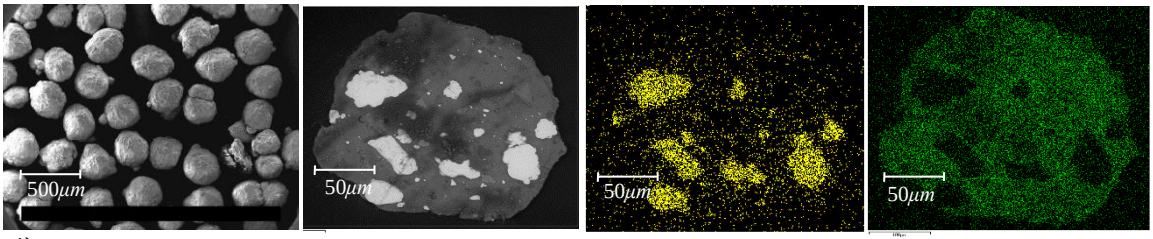

Figure 8: Cu25Ca75 i) High-resolution SFEG image (scale 500 μm), ii) Global particle view EDX, iii) Cu elemental mapping EDX, iv) Ca elemental mapping EDX

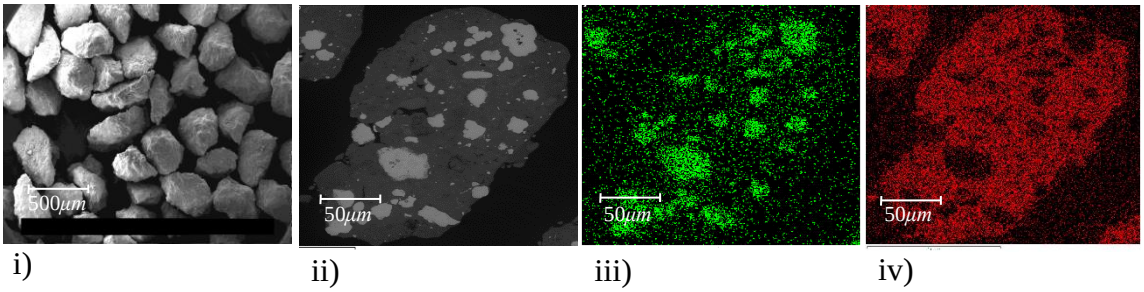

Figure 9: Cu50Ca50 i) High-resolution SFEG image (scale 500 μm), ii) Global particle view EDX, iii) Cu elemental mapping EDX, iv) Ca elemental mapping EDX

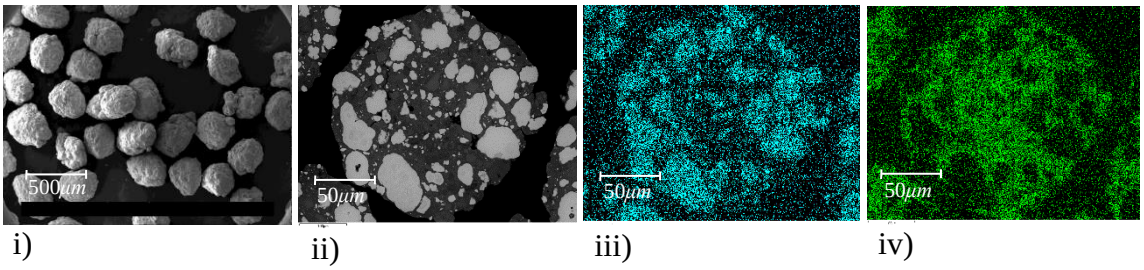

Figure 10: Cu75Ca25 i) High-resolution SFEG image (scale 500 μm), ii) Global particle view EDX, iii) Cu elemental mapping EDX, iv) Ca elemental mapping EDX

3.2 Carbon monoxide conversion

The cyclic redox behaviours of the Al300-supported oxygen carriers were assessed in a fluidised bed with twenty-five alternating oxidation (O_2 5%), reduction (CO 10%) and inert cycles at a temperature of 950 °C. The CO conversion (γ_{CO}) as a function of oxygen carrier conversion in the reduction stage (X_{red}, CuO-Cu) is shown in Figure 11 for Al300-supported oxygen carriers. The oxidising phase was sufficiently fast, and the length of the time of this period (360 s) ensured and assumes full oxidation. In all the investigations, the reduction step was sufficiently fast to ensure that the CO was fully converted by the oxygen carrier, thereby successfully reducing the active phase CuO to Cu. This is confirmed by all the oxygen carriers reaching a solid reduction conversion (X_{red}, CuO-Cu) >0.9. Comparing each specific oxygen carrier, the shape of the curve changes in relation to the degree of CO conversion and reducibility of the carrier. This is fairly indicative of the content of active CuO present. An

increase in activation or deactivation with accumulating redox cycles can be seen where the gas yield becomes reduced or increases with the effect of accumulating cycles. The general trend is followed throughout the investigation where the increased content of active CuO gives an increased CO conversion yield. The general shapes of the curves for each of the oxygen carriers become increasingly horizontal, with a CO conversion yield closer to unity indicating greater conversion of CO to CO_2 with increased CuO content. In cycle 1 of Cu75Al25 (Figure 11c), it can be concluded that the entirety of CO entering the fluidised bed in the reduction period was converted to CO_2. All of the Al300-supported oxygen carriers follow a trend whereby the primary redox cycle exhibits the greatest CO conversion. The produced gas yield is reduced as the redox cycles increase. In Cu25Al75 there is little difference between the curves in cycle 12 and 25, but both show decreased gas yield compared to the first cycle. It can be observed from the curves of Cu50Al50 and Cu75Al25 that there is a greater difference between cycle 12 and 25, which results in a reduced CO conversion yield. Cu25Al75 was the only oxygen carrier to not suffer from agglomeration. Due to the full reduction to elemental Cu, in all of the Al300-supported oxygen carriers, the particles with 50% and higher CuO suffered significant agglomeration, indicated by a drop in differential pressure during the cyclic investigations and subsequent visual inspection. Comparisons using high-resolution SEM images of the morphology between Al300-supported fresh prepared particles and those having undergone redox investigations are shown in Figures 12-14.

a)

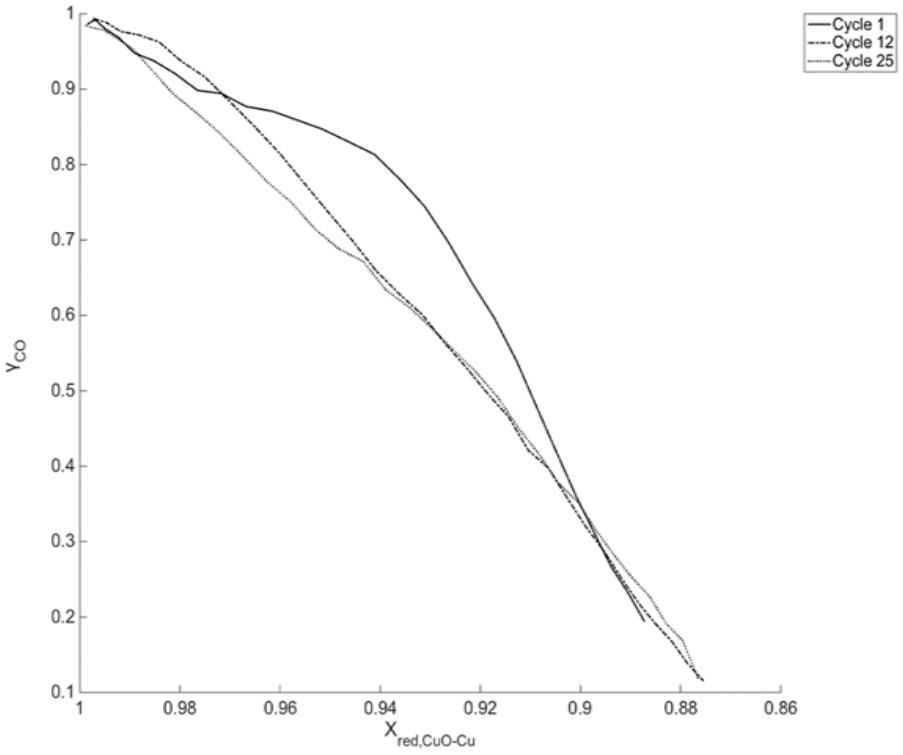

b)

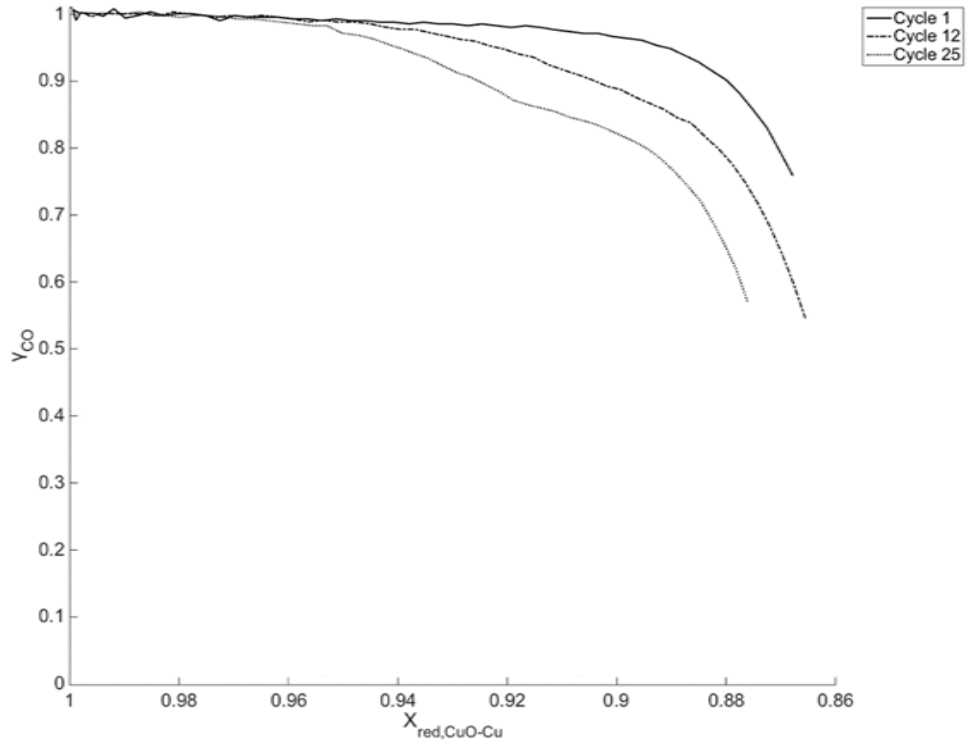

c)

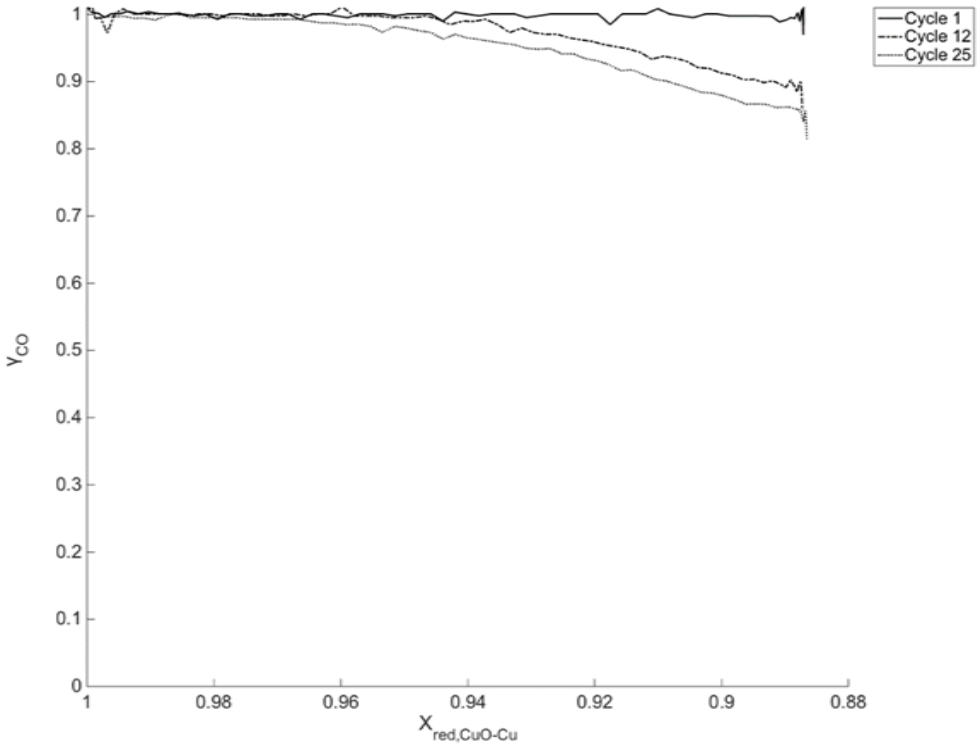

F*igure 11: Redox cyclic behaviour over 25 cycles assessed by oxygen carrier conversion vs. the conversion of CO to* CO_2*: a) Cu25Al75, b) Cu50Al50, c) Cu75Al25*

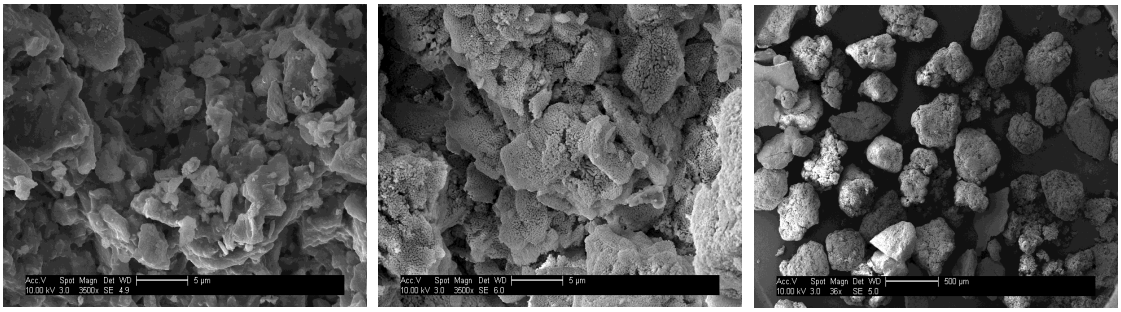

Figure 12: High-resolution SEM images showing morphology of Cu25Al75: (left) Fresh produced 5 μm; (centre) After 25 redox cycles with CO 5 μm; (right) Multiple particles after 25 redox cycles with CO 500 μm

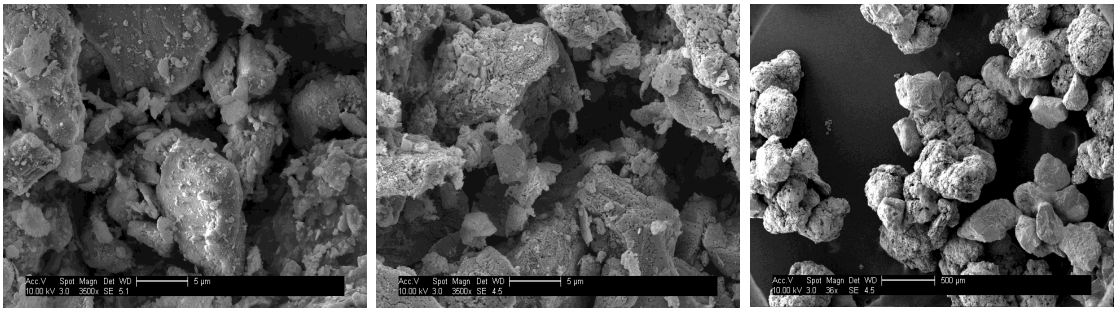

Figure 13: High-resolution SEM images showing morphology of Cu50Al50: (left) Fresh produced 5 μm; (centre) After 25 redox cycles with CO 5 μm; (right) Multiple particles after 25 redox cycles with CO 500 μm

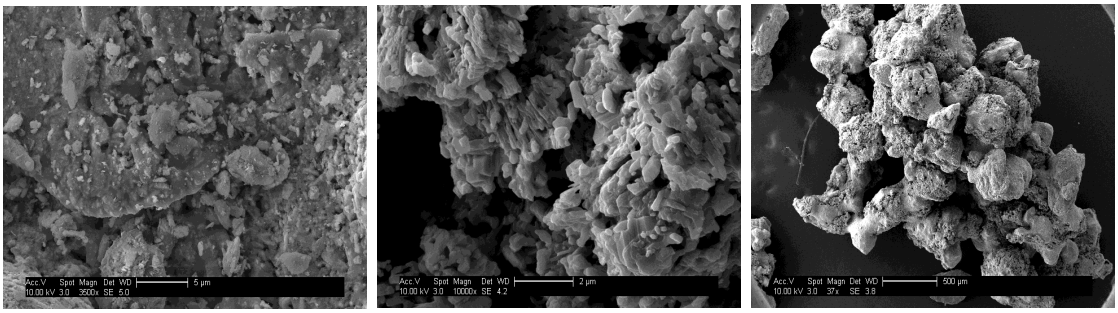

Figure 14: High-resolution SEM images showing morphology of Cu75Al25: (left) Fresh produced 5 μm; (centre) After 25 redox cycles with CO 5 μm; (right) Multiple particles after 25 redox cycles with CO 500 μm

The SEM images of the Cu50Al50 and Cu75Al25 (Figures 13 and 14) taken at x36 magnification at a scale of 500 μm of multiple particles (right) show the extent of the agglomeration of the particles, which is clearly more severe for oxygen carriers with a higher CuO content. The agglomeration would be detrimental in a circulating fluidised bed process. The general comparison of the morphology between the fresh particles and those subjected to the redox cycles shows increased pore size. The decrease in the ability to convert fuel with increasing redox cycles may have been due to particle agglomeration. A negligible decrease in CO conversion was observed in redox cycles 12 and 25 in Cu25Al75, which did not agglomerate. This leads us to conclude that agglomeration may bear an influence on the reduction in CO conversion and reaction behaviour over increasing redox cycle numbers and increased Cu content. The SEM analysis (Figures 12-14) also shows pore development. Freshly produced oxygen carrier particles exhibit a micro-porous structure which then develops into macro-pores as observed following the 25th redox cycle. This could limit the conversion of CO to CO_2 and in conjunction with the occurrence of agglomeration, therefore exhibit reaction profiles that follow the trend for decreasing gas conversion with accumulative cycles, especially for samples with 50 and 75 % wt. Cu content. Fine particulates were recovered at the filter inlet and are an indication of attrition of the oxygen carriers. Cu25Al75 particles attrite the most with losses of 7.7%. By contrast, Cu50Al50 and Cu75Al25 represented losses of 2.7% and 0.25%, respectively.

The cyclic redox behaviour of CaO-supported oxygen carriers is as shown in Figure 15. The CaO-supported oxygen carriers follow the same trend as the alumina-based Al300-supported oxygen carriers where the extent of fuel conversion appears largely due to the ratio of active CuO present in the oxygen carrier. For Cu25Ca75 and Cu50Ca50, the effect of increased fuel conversion with accumulating redox cycles is not as strongly evident as it is in the Al300-supported oxygen carriers. The Cu25Ca75 oxygen carrier improves in reducibility and yield of gas conversion with an increase in redox cycle number. For Cu50Ca50 there is a negligible difference in both reducibility of the oxygen carrier and gas conversion between different cycles. By contrast, for the Cu75Ca25 oxygen carrier, the effect of subsequent redox cycles is apparent. Here, the ability to convert CO to CO_2 is reduced when compared to the 1st and 12th redox cycles. This oxygen carrier is also subjected to severe agglomeration and can be seen in Figure 18, whereas agglomeration, which was observed in the other CaO-supported oxygen carriers, shown in Figures 16 and 17 for Cu25Ca75 and Cu50Ca50, did not occur to the same extent and did not cause de-fluidisation during the testing period.

a)

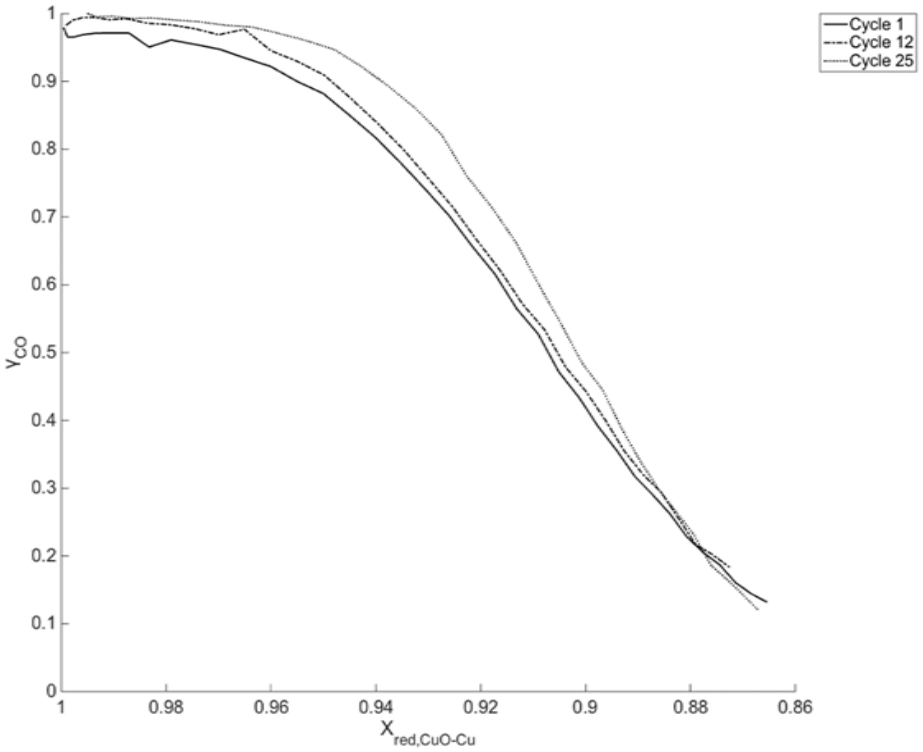
Cycle 1
Cycle 12
Cycle 25
y_{CO}
$X_{red,CuO-Cu}$
1
0.9
0.8
0.7
0.6
0.5
0.4
0.3
0.2
0.1
0
1
0.98
0.96
0.94
0.92
0.9
0.88
0.86

b)

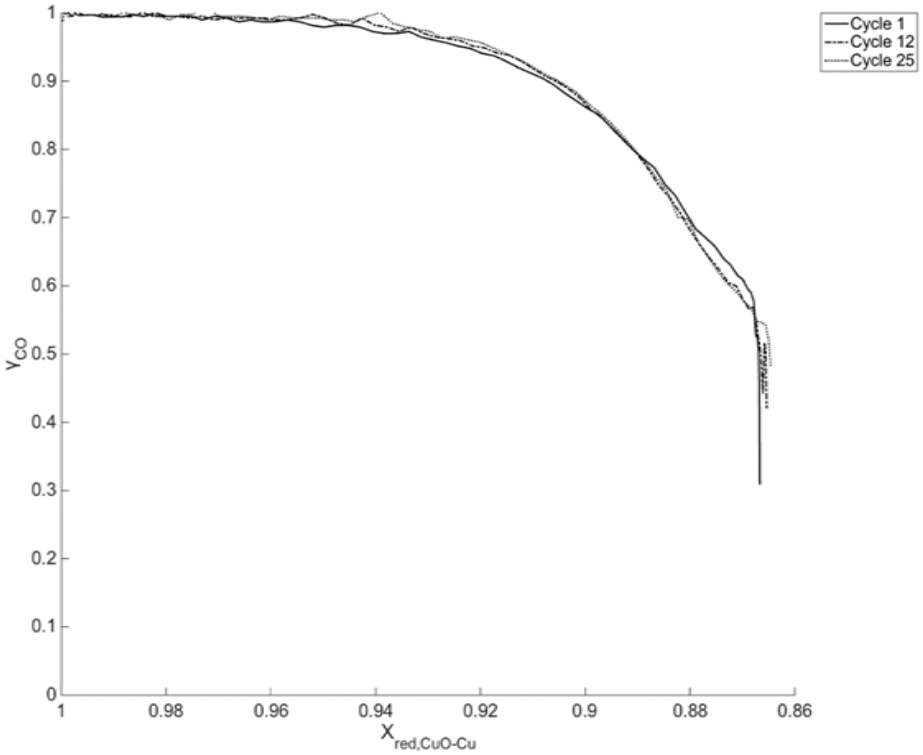
Cycle 1
Cycle 12
Cycle 25
y_{CO}
$X_{red,CuO-Cu}$
1
0.9
0.8
0.7
0.6
0.5
0.4
0.3
0.2
0.1
0
1
0.98
0.96
0.94
0.92
0.9
0.88
0.86

c)

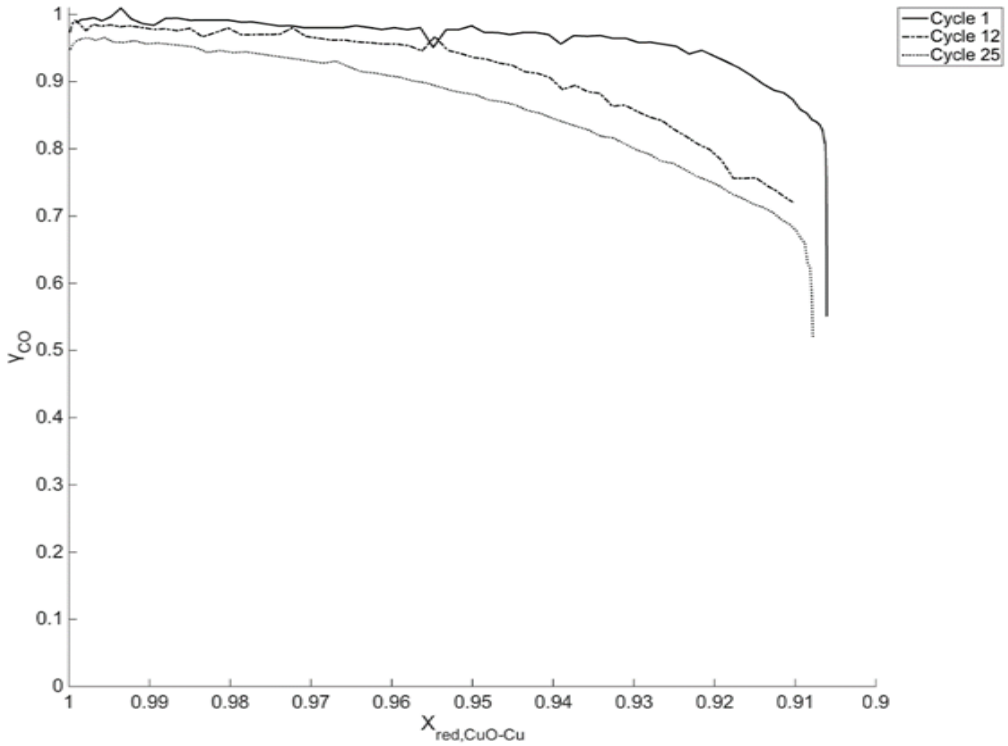

Figure 15: Redox cyclic behaviour over 25 cycles assessed by oxygen carrier conversion vs. the conversion of CO to CO_2: a) Cu25Ca75, b) Cu50Ca50, c) Cu75Ca25

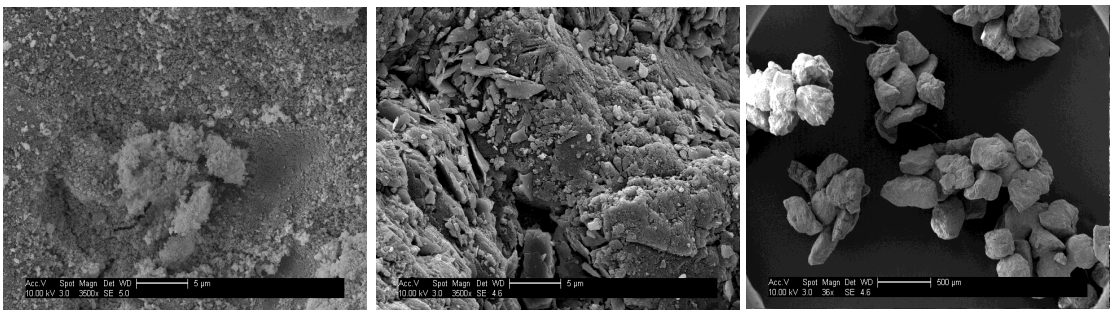

Figure 16: High-resolution SEM images showing morphology of Cu25Ca75: (left) Fresh produced 5 μm; (centre) After 25 redox cycles with CO 5 μm; (right) Multiple particles after 25 redox cycles with CO 500 μm

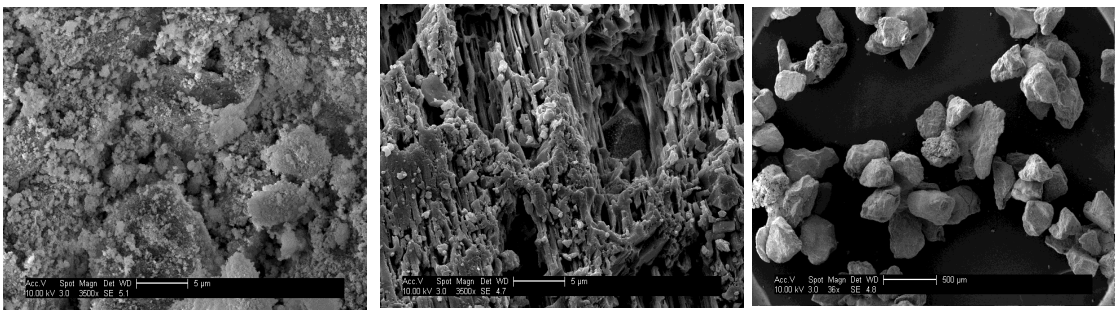

Figure 17: High-resolution SEM images showing morphology of Cu50Ca50: (left) Fresh produced 5μm; (centre) After 25 redox cycles with CO 5 μm; (right) Multiple particles after 25 redox cycles with CO 500 μm

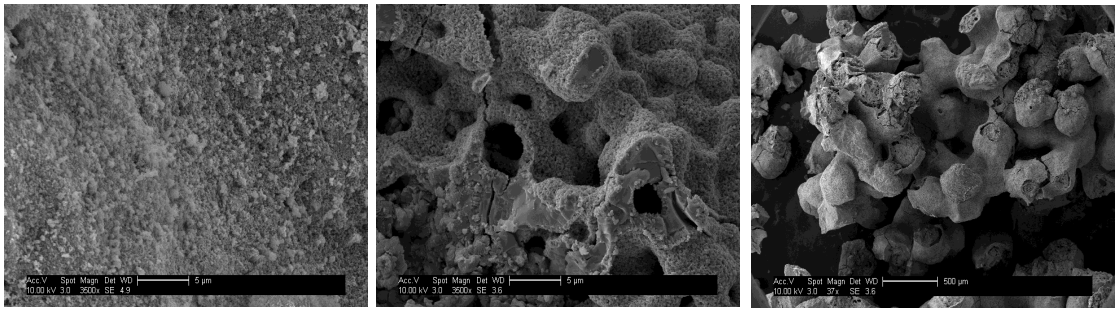

Figure 18: High-resolution SEM images showing morphology of Cu75Ca25: (left) Fresh produced 5μm; (centre) After 25 redox cycles with CO 5 μm; (right) Multiple particles after 25 redox cycles with CO 500 μm

The changes in pore structure and morphology for the CaO-supported oxygen carriers are shown in the left and centre images in Figures 16-18. The effect of the accumulative redox cycles is significant. Agglomeration is clearly present in the Cu75Ca25 oxygen carrier and can be attributed to the forming of copper-calcium phases which possess low melting points [9]. It can be observed in all the CaO-supported oxygen carriers that there is an increase in

porosity, where the micro-pores in the fresh samples developed into macro-pores in the used particles. This effect can initially give rise to greater gas diffusion in the oxygen carrier, allowing a greater surface area for gas conversion to take place [21] and is observed in the Cu25Ca75 sample. However, the formation of the macro-pores eventually leads to a reduction in surface area, and thus a reduced conversion rate, as seen in the Cu75Ca25 oxygen carrier. Again, similarly to Cu75Al25, the increased Cu content causes these samples to suffer from agglomeration, which, in conjunction with the increased pore development, causes a reduction in gas conversion with accumulative cycles. The CaO-supported oxygen carriers exhibited no significant attrition, as measured from the fines collected at the particulate filter.

3.3 Methane conversion

Cu25Al75 and Cu25Ca75 are chosen here as the most suitable oxygen carriers for a redox investigation with methane as the reducing gas, following the cyclic experiments for the conversion of CO. These oxygen carriers showed minimal agglomeration. The redox behaviour of the two oxygen carriers with methane is shown in Figure 19 and follows the trends seen in the CO conversion set of experimental investigations. It is observed that Cu25Al75 is further reduced and exhibits a higher conversion of methane in comparison to Cu25Ca75. The methane conversion yield for Cu25Ca75 is minimal and ranges between 15-25%. The curve shows that the reducibility of this oxygen carrier from CuO to Cu is also limited. The conversion of Cu25Al75 oxygen carrier to Cu was greater in extent in comparison to Cu25Ca75 (approximately 50%). The conversion of CH_4 is not complete but comparable to the conversion exhibited by highly engineered oxygen carriers described in previous literature [22]. Similarly to the reduction with CO, Cu25Al75 shows a decrease in its performance for reducibility and methane conversion with accumulating redox cycles. This is not observed in Cu25Ca75, where the effect of increasing redox cycles improves these properties, as can be seen in the comparison of the higher methane conversion yield between the 25^{th} and 1^{st} redox cycle.

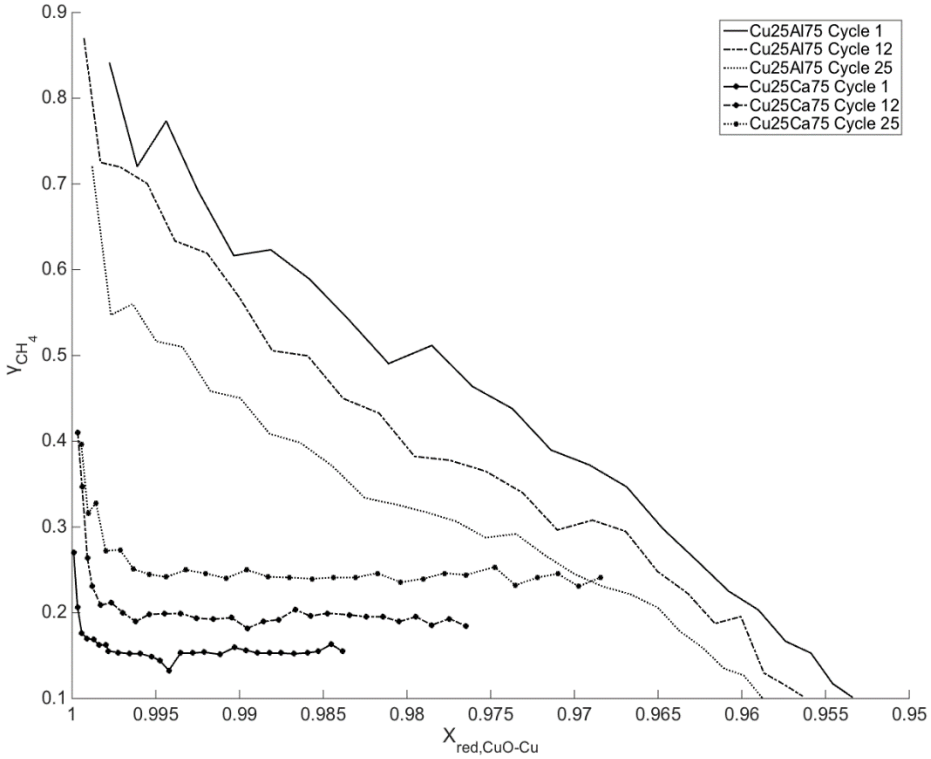

Figure 19: Redox cyclic behaviour of Cu25Al75 and Cu25Ca75 over 25 cycles assessed by oxygen carrier conversion vs. the conversion of CH_4 to CO_2

4 Conclusions

This series of experiments investigates the application of oxygen carriers for gaseous fuel conversion produced by the scalable pelletisation method utilising low-cost support materials. Copper (II) oxide in varying ratios was combined with either alumina-based cement, or CaO derived from limestone as support material in order to investigate the possible mechanical and chemical improvements. The oxygen carriers containing a greater ratio of support material are found to have enhanced crushing strength. Oxygen carriers comprised of a 1:3 ratio of support to active CuO showed increased crushing strength by a minimum of 280% compared to a pure pelletised CuO. Elemental analysis shows the distribution of CuO and support material in an oxygen carrier particle was fairly uniform, but is highly dependent on the size ranges of the materials used in the production process.

In the fluidised bed investigations, all oxygen carriers exhibit a high CO conversion yield and are fully reducible from CuO to Cu. In the Al300-supported oxygen carriers the initial redox cycle has the greatest fuel and oxygen carrier conversion. The general trend saw a decline in conversion as accumulating redox cycles are performed. In the CaO-supported oxygen carriers, this trend is not observed except for Cu75Ca25. This leads to the conclusion that the deactivation over increasing redox cycle numbers is more likely due to the deactivation of the CuO active material as well as its interaction with the Al300 support. All but one of the oxygen carriers suffered agglomeration, and the agglomeration was, as expected, more evident in carriers with higher ratios of CuO. Oxygen carrier Cu25Al75, which did not suffer

from agglomeration, showed the greatest attrition, with a loss of approximately 8% of its initial mass through the 25-redox-cycle investigation. The reduction with methane produced a decreased reducibility of the oxygen carriers and gas conversion was limited to 15-25% and 50% for Cu25Ca75 and Cu25Al75, respectively. Cu25Ca75 demonstrated improved conversion, where Cu25Al75 experienced a decrease in conversion with increasing redox cycles, although its oxygen carrier and fuel conversion was consistently greater than that of Cu25Ca75.

The pelletisation method used in this investigation is an extremely effective method for producing oxygen carrier materials, but its success strongly depends on the amount and type of materials used. The use of support material with Cu-containing oxygen carriers is crucial to its potential long-term use in chemical looping. The investigation shows that Al300 support material offers a feasible option for further long-term stability testing when active Cu content is kept below 25%.

5 Acknowledgments

The experimental investigation was conducted in part at the Centre for CCS and Combustion at Cranfield University and the Department of Engineering at Cambridge University. The authors would like to acknowledge the following for their contributions in material supply in this research investigation. Gareth Williams (Johnson Matthey) for the supply of Copper (II) Oxide, Doris Van Garsel (Almatis GmbH) for the supply of Alphabond 300 and Liam Barkley (Longcliffe) for the supply of limestone.

6 References

[1] A. Lyngfelt, B. Leckner, T. Mattisson, Chem. Eng. Sci. 56 (2001) 3101–3113.

[2] E. Jerndal, T. Mattisson, A. Lyngfelt, Chem. Eng. Res. Des. 84 (2006) 795–806.

[3] P. Moldenhauer, M. Rydén, T. Mattisson, A. Hoteit, A. Jamal, A. Lyngfelt, Energy and Fuels 28 (2014) 5978–5987.

[4] C. Linderholm, M. Schmitz, J. Environ. Chem. Eng. 4 (2016) 1029–1039.

[5] S.K. Haider, G. Azimi, L. Duan, E.J. Anthony, K. Patchigolla, J.E. Oakey, H. Leion, T. Mattisson, A. Lyngfelt, Appl. Energy 163 (2016) 41–50.

[6] J. Adánez, A. Abad, F. Garcia-Labiano, P. Gayan, L.F. de Diego, Prog. Energy Combust. Sci. 38 (2012) 215–282.

[7] A. Abad, J. Adánez, F. García-Labiano, L.F. de Diego, P. Gayán, J. Celaya, Chem. Eng. Sci. 62 (2007) 533–549.

[8] L.F. De Diego, F. García-Labiano, J. Adánez, P. Gayán, A. Abad, B.M. Corbella, J.M. Palacios, Fuel 83 (2004) 1749–1757.

[9] F. Donat, W. Hu, S.A. Scott, J.S. Dennis, Ind. Eng. Chem. Res. 54 (2015) 6713–6723.

[10] P. Gayán, I. Adánez-Rubio, A. Abad, L.F. De Diego, F. García-Labiano, J. Adánez, Fuel 96 (2012) 226–238.

[11] C.Y. Sim, T. Brown, Q. Chen, V. Sharifi, J. Swithenbank, J. Dennis, S. Scott, Chem. Eng. Sci. 69 (2012) 211–224.

[12] X. Zheng, L. Che, Y. Hao, Q. Su, J. Energy Chem. 25 (2016) 101–109.

[13] Q. Imtiaz, D. Hosseini, C. Müller, Energy Technol. 1 (2013) 633–647.

[14] H. Leion, T. Mattisson, A. Lyngfelt, Energy Procedia 1 (2009) 447–453.

[15] E.M. Eyring, G. Konya, J.S. Lighty, A.H. Sahir, A.F. Sarofim, K. Whitty, Oil Gas Sci. Technol. 66 (2011) 209–221.

[16] L. Duan, D. Godino, V. Manovic, F. Montagnaro, E.J. Anthony, Energy Technol. Submitted (2016).

[17] L.-S. Fan, Chemical Looping Systems for Fossil Energy Conversions, Wiley, 2010.

[18] M. Erans, T. Beisheim, V. Manovic, M. Jeremias, K. Patchigolla, H. Dieter, L. Duan, E. Anthony, Faraday Discuss. (2016).

[19] V. Manovic, Y. Wu, I. He, E.J. Anthony, Environ. Sci. Technol. 46 (2012) 12720–12725.

[20] P. Hallberg, D. Jing, M. Rydén, T. Mattisson, A. Lyngfelt, Energy & Fuels 27 (2013) 1473–1481.

[21] C. Qin, J. Yin, B. Feng, J. Ran, L. Zhang, V. Manovic, Appl. Energy 164 (2016) 400–410.

[22] S. Penthor, F. Zerobin, K. Mayer, T. Pröll, H. Hofbauer, Appl. Energy 145 (2015) 52–59.